ACS APPLIED MATERIALS & INTERFACES

www.acsami.org

Forum Article

Unveiling the Interfacial and Structural Heterogeneity of $Ti_3C_2T_x$ MXene Etched with CoF_2/HCl by Integrated *in Situ* Thermal Analysis

Cody B. Cockreham, Xianghui Zhang, Jeffrey A. Eakin, Martinus Dewa, Houqian Li, Nan Li, Junming Sun, Su Ha, Cornelius F. Ivory, Yong Wang, Hongwu Xu, and Di Wu*

Cite This: *ACS Appl. Mater. Interfaces* 2021, 13, 52125–52133

Read Online

ACCESS | Metrics & More | Article Recommendations | Supporting Information

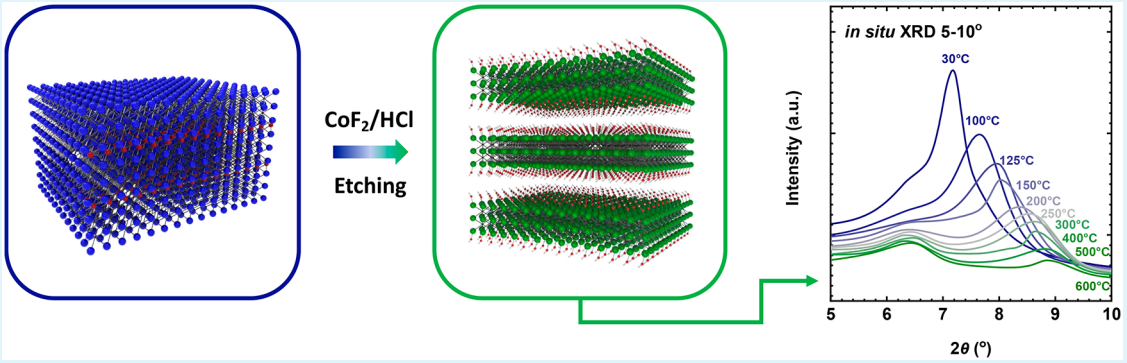

ABSTRACT: $Ti_3C_2T_x$ MXene is a member of the recently discovered two-dimensional early transition metal carbide and nitride family of MXenes with potential applications in energy storage and heterogeneous catalysis at elevated temperatures. Here, we apply a suite of *in situ* techniques to probe $Ti_3C_2T_x$ MXene's thermal evolutions, including *in situ* X-ray diffraction (XRD), *in situ* diffuse reflectance infrared Fourier transform spectroscopy (DRIFTS), and integrated thermogravimetry–differential scanning calorimetry–mass spectrometry (TG-DSC-MS). In light of this set of *in situ* investigations, we find heterogeneity in the layering of $Ti_3C_2T_x$ MXene revealed only at higher temperatures. Our findings present behavior up to 600 °C, particularly interlayer water and −OH surface end-capping groups. In one group of layers, their interlayer spacing shrinks as water deintercalates, but the other group of layers unexpectedly shows no change in the interlayer spacing. This is strong evidence that intercalants act as guest pillaring agents in the latter layering group, which stabilize these layers at higher temperatures while keeping the interlayer space accessible.

KEYWORDS: *MXenes, 2D layered materials, heterostructure, interlayer heterogeneity, in situ XRD, thermal analysis, cobalt fluoride*

INTRODUCTION

MXene is a synthetic clay-like material family of early transition metal carbides and nitrides.[1] Owing, especially, to MXene's nanolayered structure with ample interlayer space, this family demonstrates a potential application in a variety of fields such as energy storage, catalysis, environmental remediation, and electromagnetic shielding.[2−7] MXene is of the form $M_{n+1}X_nT_x$, where M is an early transition metal such as Ti or V, X is C or N, and T_x is a capping end group (−F, −OH, =O, etc.). $M_{n+1}X_nT_x$ MXene is synthesized by the selective etching of the $M_{n+1}AX_n$MAX phase, where A is most commonly Al or Ga.[8] The $Ti_3C_2T_x$ MXene is investigated here because it is the most widely researched and the first discovered.[8,9] To enable MXenes' applicability and scalability in a broad range of environments, it is imperative to understand the physicochemical properties of their interfaces and structures under processing and operation conditions as temperature varies.

Synthesized by etching with various aqueous solutions, the interfacial and structural phenomena of MXenes revealed by thermal treatments are rich. Recently, Seredych et al. investigated the thermal behavior of $Ti_3C_2T_x$, Mo_2CT_x, and Nb_2CT_x synthesized in various acidic environments using thermogravimetry coupled with mass spectrometry (TG-MS) with a particular interest in determining the effect of synthesis on surface chemistry.[10] Different etchants and etchant concentrations led to distinctive surface functional groups and different degrees of interlayer hydration; however, regardless of the surface chemistry of $Ti_3C_2T_x$, its decomposition temperatures remained similar. Their mass spectrom-

Special Issue: Emerging Materials for Catalysis and Energy Applications

Received: May 30, 2021
Accepted: August 2, 2021
Published: August 13, 2021

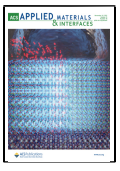

https://doi.org/10.1021/acsami.1c10021
ACS Appl. Mater. Interfaces 2021, 13, 52125–52133

etry results evidenced two types of surface-bonded water, loosely confined interlayer water species and more tightly bonded interlayer water molecules. In parallel, Thakur et al. reported an investigation into thermal evolutions of V_2CT_x with a focus on surface bonding using *in situ* Raman spectroscopy and *ex situ* X-ray diffraction (XRD), X-ray photoelectron spectroscopy (XPS), and scanning electron microscopy (SEM).[11] Their study suggested thermal dehydration led to a decrease in interlayer space. Other studies have investigated the thermal stability of MXenes such as Ti_2CT_x, V_2CT_x, $Ti_3C_2T_x$, and $Ti_3C_2T_x$/composites using a combination of differential scanning calorimetry (DSC) and thermogravimetry (TG).[12,13,22,14−21] The general phenomena are interlayer water loss between 100 and 250 °C, the loss of surface groups between 600 and 900 °C, and finally total decomposition between 800 and 1100 °C. The studies investigating the thermal stability of $Ti_3C_2T_x$ MXene have been etched in different environments (i.e., HF or NH_4HF_2).[10,13,14,22] In summary, it was found that the properties of MXenes under thermal treatments are strongly dependent on their composition and surface chemistry determined by the etching environment. The synthesis and performance of MXenes have been extensively studied. To our knowledge, thus far, systematic investigation into the interfacial, structural, and thermal evolutions of MXenes as temperature varies using *in situ* methods under a controlled gas atmosphere is rarely performed. Understanding the thermal and structural responses as well as the bonding evolution *in situ* or in *real time* as a function of temperature is essential and critical as the MXene materials might undergo a wide range of temperatures in the actual processing or a working environment.

In this study, we present integrated research using *in situ* experimental approaches to reveal the structural evolutions, interfacial phenomena, and thermal pathways of $Ti_3C_2T_x$ MXene at elevated temperatures in which *in situ* XRD with *in situ* diffuse reflectance infrared Fourier transform spectroscopy (*in situ* DRIFTS) and TG-DSC-MS were systematically coupled. The $Ti_3C_2T_x$ MXene sample used here is uniquely synthesized in a CoF_2/HCl etching environment from its parent Ti_3AlC_2 MAX we reported earlier.[23] Moreover, we investigate its structure, morphology, and atomic microstructure using *ex situ* XRD, SEM, and high-resolution transmission electron microscopy (HRTEM) to support conclusions from *in situ* experiments and simultaneous thermal analysis. Our results suggest that CoF_2/HCl etching leads to layered intercalated water, a heterogeneous internal surface, and surprisingly, simultaneous formation of intercalated guest species acting as pillaring agents, which support a large MXene interlayer distance even at high temperatures after complete interlayer dehydration and dehydroxylation.

EXPERIMENTAL METHODS

Synthesis of $Ti_3C_2T_x$ by CoF_2/HCl Etching. Ti_3AlC_2 MAX phase with a reported mean particle size of ∼800 nm was purchased from Luoyang Tongrun Info Technology Co., Ltd. 1g of Ti_3AlC_2 corresponding to 4.3 wt % was added to 20 mL of 6 M HCl, prepared from 37 wt % HCl (Sigma-Aldrich), and mixed in a 50 mL polypropylene test tube. 1.75 g of CoF_2 (Sigma-Aldrich) corresponded to a molar ratio of 3.6 CoF_2 to Ti_3AlC_2. The solution was mixed for 30 s using a test tube agitator and then put into the bath sonicator for 30 min. After which, the mixture was heated to 60 °C for 48 h. The suspension was washed with copious amounts of deionized water over a vacuum filtration system and left to dry for 12 h. The powder was collected and dried overnight in vacuum at ∼60 °C.

***Ex Situ* Powder X-ray Diffraction (XRD) and Compositional Analyses.** Phase analysis of CoF_2 etched $Ti_3C_2T_x$ MXene was performed by *ex situ* powder X-ray diffraction (*ex situ* XRD). *Ex situ* XRD data was obtained using a Rigaku Smartlab with Cu Kα radiation (k = 1.5406 Å) operated at a scan rate of 4°/min in the 2θ range of 5−80°. The elemental composition of Al, Co, and Ti was measured using an Agilent 5100 inductively coupled plasma optical emission spectrometer (ICP-OES). Samples were prepared by dissolving samples in 35 wt % HNO_3 at room temperature before diluting to 2 wt % HNO_3.

Electron Microscopy (EM). The morphology was examined using scanning electron microscopy (SEM; Quanta 200F) in the Franceschi Microscopy and Imaging Center at Washington State University and high-resolution transmission electron microscopy (HRTEM; FEI Titan 80-300 TM with a monochromator, image aberration corrector, and a PHENIX energy dispersive X-ray spectrometer detector) at Los Alamos National Laboratory. *ImageJ* (NIH) was employed for micrograph analysis.[24]

Thermal Analysis. The thermal analyses using integrated TG-DSC-MS were carried out on a Netzsch Instrument STA 449 F3 Jupiter coupled to a QMS 403 D Aëolos quadrupole mass spectrometer. The instrument has a temperature resolution of 0.001 K, a DSC resolution of 1 μW, an enthalpy accuracy of 1% measured with indium, and a balance resolution of 0.1 μg. In each measurement, about 20 mg of powder sample was analyzed in an alumina crucible from 40 to 1000 °C at 10 °C/min under gas flow, either nitrogen or air. The evolved gases of the TG-DSC experiments were identified simultaneously by the coupled MS. The data were analyzed using the Proteus and Dispsav software packages. MS, DTG, and DDSC curves were smoothed in Origin using the Adjacent-Average method with 5 points. This system was also used in our earlier studies on MXenes, shale rocks, zeolites, and layered double hydroxides (LDHs).[23,25−27]

***In Situ* Diffuse Reflectance Infrared Fourier Transform Spectroscopy (*in situ* DRIFTS).** Infrared spectra were obtained at 4 cm^{-1} resolution between 4000 and 600 cm^{-1} using a Bruker Tensor 27 FTIR spectrometer. 128 scans were used for each spectrum. KBr was used to get the background at each temperature. About 20 mg of sample (mixture of KBr and sample at a weight ratio of KBr/sample = 10:1) was used. The sample was ramped to different temperatures (50, 100, 150, 200, 250, 300, 350, and 400 °C) at 10 °C/min with a hold time of 5 min under a flow of 50 mL/min helium.

***In Situ* X-ray Diffraction (*in situ* XRD).** The structural evolution from heat treatment was characterized by *in situ* powder X-ray diffraction (*in situ* XRD). XRD data were obtained using a Rigaku Smartlab with Cu Kα radiation (k = 1.5406 Å) coupled with an Anton Paar XRK 900 furnace operated at a scan rate of 4°/min in the 2θ range of 5−65° with a heating rate of 10 °C/min under 50 mL/min of helium with hold times of 5 min before measurement.

RESULTS

Complete etching of $Ti_3C_2T_x$ MXene using CoF_2/HCl was ensured by *ex situ* XRD (see Figure 1). The patterns of etched $Ti_3C_2T_x$ MXene suggest complete conversion to MXene from the MAX phase seen by displaying representative $Ti_3C_2T_x$ MXene peaks at 2θ ∼ 7° and 61° as well as the removal of Ti_3AlC_2 MAX phase peaks at ∼34°, 39°, and 42°. Small amounts of the $AlF_3{\cdot}3H_2O$ byproduct are present, indicated by the 2θ peak at ∼17°.[23] According to ICP-OES analysis, CoF_2/HCl etched $Ti_3C_2T_x$ MXene contains significant Al^{3+}, showing an average Al/Ti ratio of ∼0.07. No residual Co-containing species from the synthesis was detected. Complete ICP-OES analysis data is presented in Table S1.

The morphological features were examined by SEM (see Figure 2a). CoF_2/HCl etched $Ti_3C_2T_x$ MXene presents the expected layered book-like morphology, further supporting the *ex situ* XRD analysis of complete etching.[23] The atomic-scale microstructure of the MXene sample is revealed by the HRTEM image in Figure 2b. Interestingly, there appears to be

https://doi.org/10.1021/acsami.1c10021
ACS Appl. Mater. Interfaces 2021, 13, 52125−52133

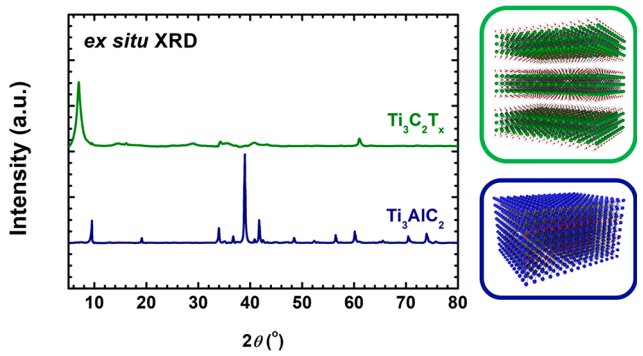

Figure 1. Structures and *ex situ* X-ray diffraction (XRD) patterns of CoF_2/HCl etched $Ti_3C_2T_x$ MXene (upper right: Ti, green; C, gray; O, red; H, white) and its parent Ti_3AlC_2 MAX phase (lower right: Ti, navy; C, gray; O, red; H, white).

darker ovular regions, seemingly, within the interlayer space of a MXene stack. According to the *ex situ* XRD patterns, this may possibly be $AlF_3{\cdot}3H_2O$ (see Figure 1). These areas are not expected to be due to the MAX phase because the near-edge area of MXenes is etched first as etching ions enter at the openings to the layers. On the basis of the *ex situ* XRD, SEM, and TEM data, we could not determine that the aluminum fluoride species is interlayer confined or surface anchored. This will be investigated in detail with *in situ* characterizations.

The thermal evolutions and intricate interfacial interactions of the CoF_2/HCl etched $Ti_3C_2T_x$ MXene were investigated using TG-DSC-MS (shown in Figure 3a–c). Mass loss occurs in three stages. DSC and DDSC results show three endothermic calorimetric events (see Figure 3b). *Stage I* is the loss of water, approximately 0.8 wt %, loosely attached on the external surface of MXene, and mainly occurs below 100 °C. The very weak endothermic DSC peak further confirms that water–MXene interactions on the external surface are weak. *Stage II* mass loss (~2.8 wt %) occurs from 100 to 175 °C, accompanied by two overlapped endothermic calorimetric signals. According to the MS data (m/z 18), *Stage II* weight loss is due to the deintercalation of MXene's tightly bound intercalated water. The existence of a pair of overlapped peaks in the DTG, DSC, and MS profiles strongly suggests that there are two groups of energetically distinctive confined water within MXene's interlayer space exhibiting two unique dehydration phenomena in thermal analysis. Particularly, intercalated water molecules, not in the internal surface of MXene, that interact merely with the other confined water molecules through water–water intermolecular interactions are liberated first, at about 112 °C, while the more tightly bonded water close to the surface functional groups, especially –OH and –F groups, are desorbed at 149 °C (see Figure 3a–c).[23,28] *Stage III* occurs above 175 °C owing to gradual detachment of surface functional groups, such as –OH and –F.[23] To a limited degree, the decomposition of $AlF_3{\cdot}3H_2O$ and its intermediate, $AlF_3{\cdot}0.5H_2O$, to AlF_3 may also contribute to the weight loss and thermal events above 175 °C,[29] but from the XRD analysis, we expect the contribution to be minor. The TG curve does not flatten even up to 600 °C, indicating continued detachment of the surface groups. Thermal analysis results strongly suggest that, other than the bulk water on the external surface of MXene, there are two types of interlayer water species. The detachment of surface groups continues after complete dehydration at about 200 °C lasting until 600 °C. We hesitate to quantify the dehydration enthalpies of these two water–MXene interactions because of the small magnitudes of DSC peaks in Figure 3b. On the other hand, the change in sample morphology as temperature increases was also investigated using SEM and presented in Figure 4. Compared with the SEM image at room temperature in Figure 4a, after isothermally heating at 600 °C for 3 h in an inert atmosphere (see Figure 4b), $Ti_3C_2T_x$ MXene retains its book-like layered morphology with open interlayer space up to 600 °C despite a slightly smoothed surface and edges.

In situ DRIFTS spectra are presented in Figure 5. The broad peak in the range of 4000 to 3200 cm^{-1} and smaller sharper peaks around 1580 cm^{-1} indicate –OH bonding of tightly bound surface water, the intercalated water. The peak at 1580 cm^{-1} can be seen in the magnified *in situ* DRIFTS spectra presented in Figure S1. The peak at 1580 cm^{-1} vanishes at 100 °C. The broad peak from 4000 to 3200 cm^{-1} subsides and is difficult to distinguish above 100 °C. This corresponds with the loss of interlayer water. The peak at ~1390 cm^{-1} can be attributed to –OH end groups (Ti–OH).[30] The intensity of this peak decreases at 100 °C while water is actively

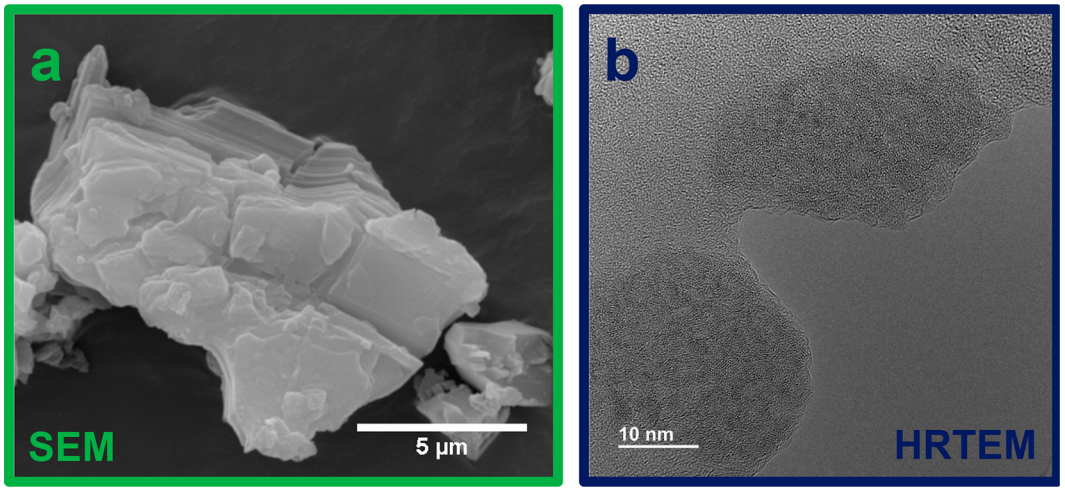

Figure 2. Morphologies of CoF_2/HCl etched $Ti_3C_2T_x$ MXene revealed by (a) scanning electron microscopy (SEM) and (b) high resolution transmission electron microscopy (HRTEM).

https://doi.org/10.1021/acsami.1c10021
ACS Appl. Mater. Interfaces 2021, 13, 52125–52133

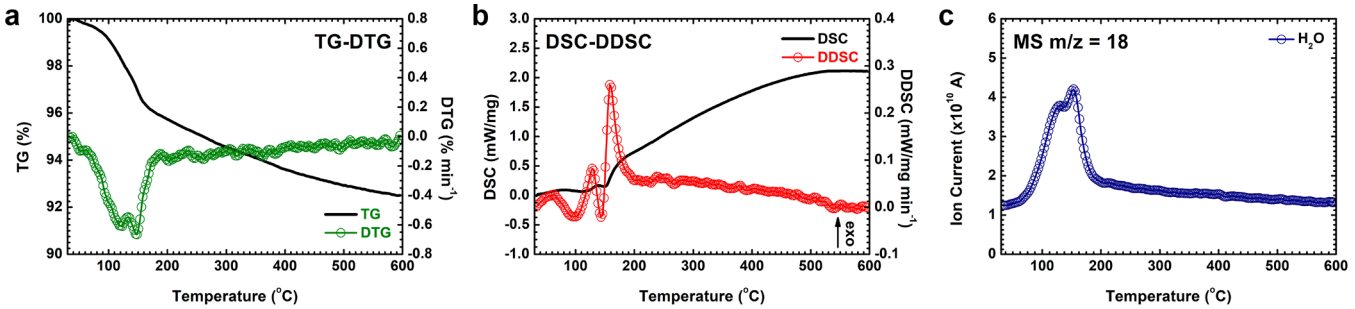

Figure 3. Thermal analysis results of CoF_2/HCl etched $Ti_3C_2T_x$ MXene in nitrogen at 10 °C/min. (a) Thermogravimetry and derivative thermogravimetry (TG-DTG), (b) differential scanning calorimetry and derivative differential scanning calorimetry (DSC-DDSC), and (c) mass spectrometry (MS) of m/z = 18.

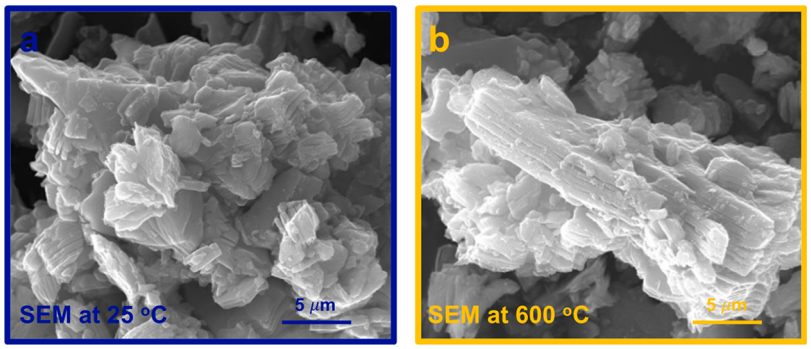

Figure 4. Scanning electron microscopy (SEM) images of CoF_2/HCl etched $Ti_3C_2T_x$ MXene (a) at room temperature and (b) after treatment at 600 °C in helium for 3 h.

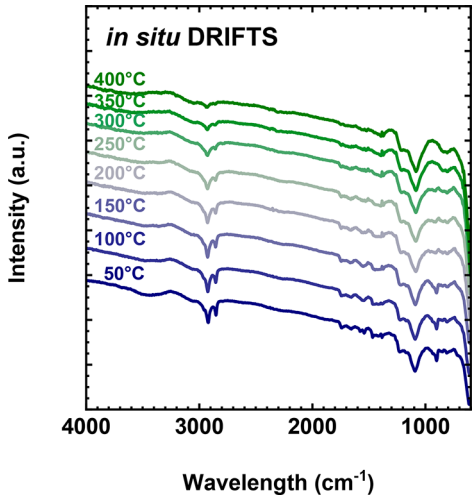

Figure 5. *In situ* diffuse reflectance infrared Fourier transform spectroscopy (DRIFTS) spectra as a function of temperature from 50 to 400 °C in helium flow (50 mL/min).

deintercalated and then reemerges at 150 °C and becomes better resolved until 250 °C. Matching the thermal analysis, most of the water loss occurs at less than 200 °C. This indicates that −OH bonded surface groups are stable only up to 400 °C and are removed below 500 °C, which implies that these hydroxyl surface groups would evolve as water, leaving behind reacted near-surface TiO_2, which is evidenced and verified as occurring at 500 °C from the structural analysis results presented below. Additionally, the IR absorbance signals between 1400 and 1000 cm^{-1} are clear evidence of C−F stretching on the MXene surface, similar to fluoro compounds. This may be evidence of Ti leaching during etching due to the harsh reaction conditions used. In sum, between 100 and 200 °C, water−surface interactions are concluded, and hydroxyl surface groups are removed at less than 500 °C.

The structure as a function of temperature was investigated using *in situ* XRD. The XRD patterns from 5° to 65° of thermally treated CoF_2/HCl etched $Ti_3C_2T_x$ MXene are shown in Figure 6. The reflection peaks of (110) and (002) correspond to *a*, interplanar unit cell distance, and *c*, interlayer unit cell distance, lattice parameters. Up to 100 °C, no detectable structural change is observed. As temperature increases, the (002) peak broadens and shifts to the right,

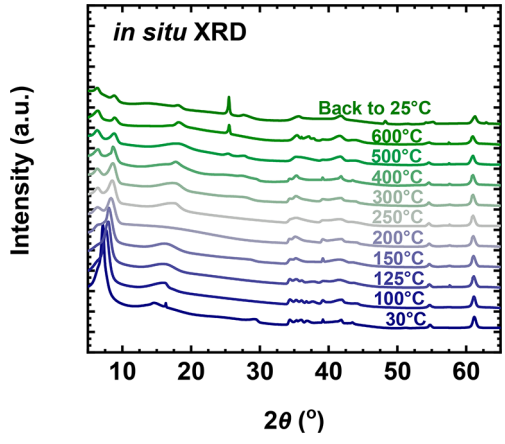

Figure 6. *In situ* X-ray diffraction (XRD) patterns of CoF_2/HCl etched $Ti_3C_2T_x$ MXene as a function of temperature from 30 to 600 °C in helium (50 mL/min), 2θ from 5 to 65°.

https://doi.org/10.1021/acsami.1c10021
ACS Appl. Mater. Interfaces 2021, 13, 52125−52133

indicating a growing distribution in interlayer spacings and a decrease in the magnitude of interlayer space. This is due to, initially, water deintercalation and, finally, loss of end-capping groups (−F, −OH, etc.) as indicated by the *in situ* DRIFTS analysis above. This trend can be seen to continue through heat treatment up to 600 °C. The simultaneous oxidation of the near-surface titanium of $Ti_3C_2T_x$ into anatase TiO_2 is apparent at 500 °C, shown by the emergence of the peak at ∼26°. This is further evidence of the loss of surface functional groups, as the oxygen to form TiO_2 must come from the sample due to the inert atmosphere (Ti−O to TiO_2 and Ti−OH to H_2O and TiO_2).

Lattice parameters as a function of temperature are presented in Figure 7. $Ti_3C_2T_x$ MXene has hexagonal closed

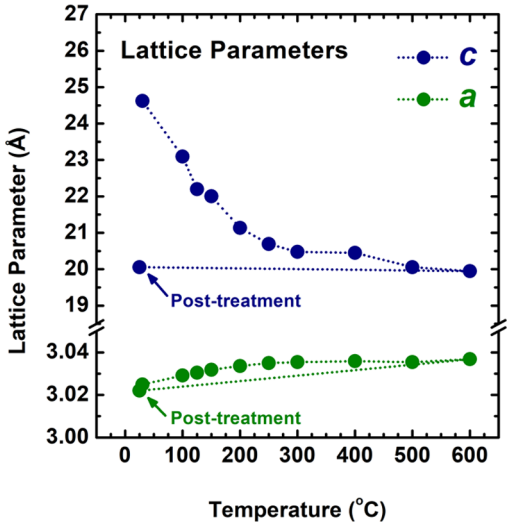

Figure 7. Lattice parameter evolutions for CoF_2/HCl etched $Ti_3C_2T_x$ MXene as a function of temperature from 30 to 600 °C in helium.

packing.[31] From 30 to 200 °C, the *c* lattice parameter, initially 24.6 Å, decreases dramatically to 21.1 Å, due to water leaving the interlayer space. The *c* lattice parameter stabilizes at 20.5 Å after residual water deintercalation after 300 °C, up to 400 °C. From 400 to 600 °C, the *c* lattice parameter further decreases to 20.0 Å as end-capping groups are removed. The *a* lattice parameter increases with temperature up to 200 °C and then remains constant. This is expected to be due to thermal expansion. Overall, the total change is minor compared to the *c* lattice parameter. Table S2 presents detailed structural information on lattice parameters and unit cell volumes for the $Ti_3C_2T_x$ MXene phase at the measured temperatures.

In Figure 8, *in situ* XRD patterns from 5° to 10° are presented to highlight the (002) peak evolution. First, it is observed that the initial (002) peak broadens and shifts to the right, as described above. The decrease in intensity of this (002) peak suggests long-range structural disorder due to the high-temperature treatment. This is attributed to the dynamic nature of water deintercalation and surface group detachment for each distinctive MXene particle. Second, most interestingly, it is apparent that there are two (002) peaks. The second (002) peak, ∼6.3°, emerges from the initial (002) peak as water deintercalates and the peak shifts to the right. The beginning of this second (002) peak can be considered as a shoulder, initially, and then emerges at 200 °C. This second (002) peak corresponding to a large *c* lattice parameter of 27.6

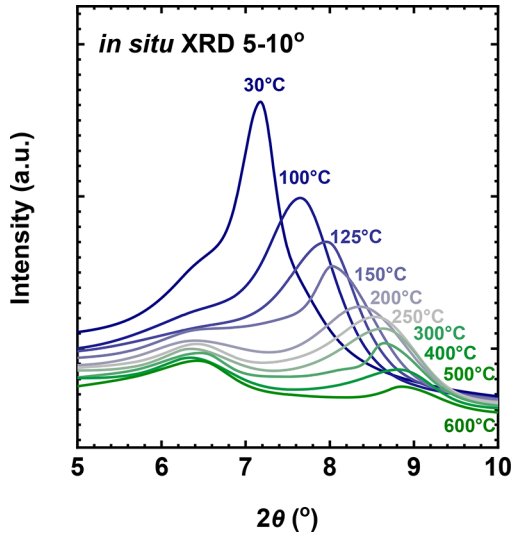

Figure 8. *In situ* X-ray diffraction (XRD) patterns of CoF_2/HCl etched $Ti_3C_2T_x$ MXene as a function of temperature from 30 to 600 °C in helium, 2θ from 5 to 10°.

Å remains constant as temperature increases. This phenomenon strongly suggests a guest species in the interlayer space acting as a pillaring agent, allowing the deintercalation of water at high temperatures with a large interlayer space. In general, the structural analysis gives us a complementary perspective into the dehydration and surface group decomposition but also points us to a new phenomenon for CoF_2/HCl etched $Ti_3C_2T_x$ MXene, which features a large interlayer space that does not change during dehydration and decomposition.

DISCUSSION

We examined the thermal stability, structural evolution, and surface bonding of $Ti_3C_2T_x$ etched in a unique CoF_2/HCl environment using integrated thermal techniques. We present a summary of the thermal behavior and then follow it with a more in-depth discussion on the details of multistep dehydration, −OH surface group detachment, and an unexpected "assemblage" of layers that retain a large interlayer spacing at high temperatures.

Stage I: 30 to 100 °C. In Stage I, the dehydration of bulk water occurs. In other words, the loosely adsorbed external surface waters are removed.

Stage II: 100 to 175 °C. Stage II results in the deintercalation of the weakly confined interlayer water and then the tightly bonded water close to and on the internal surface of MXene. Any remaining intercalated waters are removed, and −OH or −F surface groups emerge and remain stable. The sample experiences a significant decrease in the interlayer distance.

Stage III: 175 to 600 °C. In Stage III, the surface end groups detach, and −OH groups react among themselves to produce H_2O and near-surface TiO_2, leading to a relatively small decrease in interlayer distance and growing disorder in the interlayer distance intercalated guest species, leading to a pillaring phenomena.

When one considers dehydration, the majority of water loss occurs below 175 °C. From the TG-DSC-MS and *in situ* DRIFTS, it is clear that there are two types of water loss: first, the dehydration of loosely confined water having only hydrogen bonding with adjacent water molecules under

https://doi.org/10.1021/acsami.1c10021
ACS Appl. Mater. Interfaces 2021, 13, 52125−52133

confinement and, second, the removal of more tightly bound water having surface−water interactions. The study by Seredych et al. supports our findings, which evidenced two types of intercalated waters.[10] It was shown that a larger interlayer spacing was found in a 30 wt % HF etched MXene compared to a 5 or 10 wt % HF etched MXene, which exhibit smaller interlayer spacings, leading to these two distinct intercalated waters.[10,32] This is supported by our structural analysis showing two layering distances with a water bilayer (24.6 Å, room temperature) and multilayers of water (27.6 Å, revealed after heat treatment).[33−35] The prethermally treated lattice parameter values of a = 3.0 Å and c = 24.6 Å correspond well with the lattice constants determined from Na^+ and K^+ intercalated $Ti_3C_2T_x$ MXene.[31,33−35] Upon heating to 600 °C, the unintercalated $Ti_3C_2T_x$'s interlayer space decreases 4.6 Å, again implying a bilayer of intercalated water.[34] Here, water loss occurs at lower temperatures than $Ti_3C_2T_x$ etched in lower percentages of HF but has dehydration behaviors similar to $Ti_3C_2T_x$ etched in 30, 40, and 50 wt % HF.[10,14,36] This may be due to two factors. First, the presence of a more open layering seen by the large c lattice parameter leads to less tightly confined multilayer waters and, second, higher amounts of hydrophilic −OH end groups are found in lower concentration HF etchings with less hydrophilic −F groups being found in higher concentration HF etchings, such as our CoF_2/HCl environment. Supporting the existence of high amounts of −F end groups is the apparent lack of −OH groups observed in our *in situ* DRIFTS analysis. Compared with the literature, the IR spectra in Figure 5 show −OH (water) peaks with much less intensity than other reported MXene spectra.[30,37,38] Our results, combined with those of others, provide an enhanced understanding of the relationship of water within the $Ti_3C_2T_x$ MXene's layers.

From the *in situ* DRIFTS and *in situ* XRD analyses (see Figures 5−8), we can draw conclusions about the −OH surface end groups. The −OH surface groups are evidenced to detach between 400 and 500 °C. As dihydroxylation proceeds, −OH groups are expelled as H_2O and leave behind localized near-surface TiO_2. Similar to our TG-DSC-MS results, Seredych et al. (TG-MS) and others (TG) do not see a noticeable loss of −OH surface groups at such low temperatures.[10,12−15,22] For example, Seredych et al. detect functional group detachments at above 800 °C.[10] We also do not see obvious thermogravimetric or thermal events in our TG-DSC-MS. The disparity can easily be explained by the dynamic nature of the TG techniques, which undergo rapid heating, and reactions that are kinetically or mass transport limited will be shifted along to higher temperatures compared to other methods. *In situ* DRIFTS and *in situ* XRD require relatively long hold times at each temperature sampled, allowing the sample to reach equilibrium. Supporting our analysis, we find that clays, natural two-dimensional layered systems such as chlorites, halites, kaolinites, smectites, and vermiculites, dehydroxylate between 400 and 600 °C.[39,40] The removal of functional groups (−OH) results in a decrease in the interlayer spacing and overall degradation of the sample as evidenced by the formation of TiO_2 and more disordered layering, broader (002) peaks. However, after surface functional groups react and detach, the product retains its layered structure up to 600 °C. Because of MXene's variability in surface chemistry, structure, and morphology resulting from its MAX parent phase and the etching environment, many opportunities exist to study the bonding of surface groups and their thermal and thermodynamic stability.

As a consequence of investigating the effect of heat treatment on the structure, we find two different (002) peaks for the same $Ti_3C_2T_x$ MXene studied (Figure 8). This is an unexpected new finding. Water deintercalates as temperature increases; one would expect a decrease in the c lattice parameter due to a shortening of the interlayer space.[11] However, the second (002) peak at ∼6.3° remains stable when the temperature is raised. The c lattice parameter of this second (002) peak of $Ti_3C_2T_x$ MXene (27.6 Å) is similar to LiF/HCl etched "clay-like" MXene, which was reported to have a c lattice constant between 27 and 28 Å.[33−35,41] This peculiarity implies that there is pillaring/swelling action occurring from species other than water in the interlayer space. MXene devoid of intercalants including water with a mix of both −F and −OH end groups displayed a c lattice parameter of 19.86(2) Å.[31] On the basis of our compositional analysis, we reason that there is Al^{3+} species within some of the interlayer spaces left over from the etching of Ti_3AlC_2 MAX, likely to be $AlF_3 \cdot 3H_2O$. This is supported by the existence of $AlF_3 \cdot 3H_2O$ in our XRD analyses; $AlF_3 \cdot 3H_2O$ is a common byproduct that can be seen in large quantities when using a high ionic strength etching environment, such as CoF_2/HCl.[23,42] From the difference in the two interlayer spaces, we estimate the thickness of the interlayer $AlF_3 \cdot 3H_2O$ to be ∼7.6 Å. We conclude that significant interfacial and structural heterogeneity exists with our sample, given that there are two types of layering: (i) with no pillaring guest agents, which sees a systematic decrease of interlayer space with water deintercalation and surface group detachment; (ii) with a pillaring guest agent (most likely Al^{3+} species). A thermally stable pillaring action may have advantages for processes like catalysis, which require fast interlayer transport at higher temperatures. Further, using the technique of testing thermally treating MXene allows researchers to investigate intercalation actions without the interference of interlayer water. Our results raise significant questions about the composition of the pillaring agent and its relationship to $Ti_3C_2T_x$ MXene.

What is the exact composition and structure of the intercalants? Are there MXene particle groups with intercalated species in all of their layers or do they occur in some layers but not others of a particle group? Is there any order to the species within a layer?

Future work includes determining the composition of the intercalants and the relative distribution of the intercalated layers. The next rational steps consist of electron microscopy techniques to investigate the inner and outer sections of MXene to define the effect of etching as a function of distance from the edge. Using other X-ray techniques, like the pair distribution function, could help illuminate any interlayer species' structure and identity. Indeed, we are just beginning to characterize MXene at higher temperatures. The multifaceted approach presented here lays a foundation for future work investigating MXene's intercalation phenomena, heterogeneity, and thermal evolutions.

CONCLUSIONS

By investigating the thermal behavior using *in situ* techniques, we segment $Ti_3C_2T_x$ MXene etched with CoF_2/HCl into three thermal stages up to 600 °C: *Stage I*, desorption of water loosely attached on the external surface; *Stage II*, thermal dehydration of intercalated (confined) water with distinct

https://doi.org/10.1021/acsami.1c10021
ACS Appl. Mater. Interfaces 2021, 13, 52125−52133

energetic states; *Stage III*, detachment of surface functional groups and simultaneous formation of the pillaring structure. Two types of confined interlayer water (weakly confined and more strongly bonded) are uncovered, evidenced by deintercalation at different temperatures. −OH surface functional groups detach between 400 and 600 °C, implying that other functional groups (i.e., −F and =O) may also detach during this temperature range. Furthermore, during our investigation, two types of thermal behavior of the layers of our $Ti_3C_2T_x$ MXene are exhibited. From this, we surmise there exist two types of layering systems present in our sample. The layering groups are distinguished by the following: (i) an expected decrease in interlayer space as water deintercalates above 100 °C and (ii) no change in the interlayer distance due to an increase in the temperature and decrease in the interlayer water. We anticipate that this is due to Al^{3+} species, which act as stabilizing pillars, enabling robust open architecture and allowing large interlayer distances even at high temperatures. Our mapping of the evolution of our $Ti_3C_2T_x$ MXene etched with CoF_2/HCl provides insight into its thermal stability and behavior at elevated temperatures and highlights the surface complexity (2D) and intricate pillaring structure (3D) of $Ti_3C_2T_x$ MXene etched with CoF_2/HCl.

■ ASSOCIATED CONTENT

Supporting Information

The Supporting Information is available free of charge at https://pubs.acs.org/doi/10.1021/acsami.1c10021.

Compositional analysis from ICP-OES, lattice parameters calculated from *in situ* XRD, and magnified view of *in situ* DRIFTS at the peak of ∼1580 cm^{-1} (PDF)

■ AUTHOR INFORMATION

Corresponding Author

Di Wu − *Alexandra Navrotsky Institute for Experimental Thermodynamics, The Gene and Linda Voiland School of Chemical Engineering and Bioengineering, Department of Chemistry, and Materials Science and Engineering, Washington State University, Pullman, Washington 99164, United States;* orcid.org/0000-0001-6879-321X; Email: d.wu@wsu.edu

Authors

Cody B. Cockreham − *Alexandra Navrotsky Institute for Experimental Thermodynamics and The Gene and Linda Voiland School of Chemical Engineering and Bioengineering, Washington State University, Pullman, Washington 99164, United States; Earth and Environmental Sciences Division, Los Alamos National Laboratory, Los Alamos, New Mexico 87545, United States*

Xianghui Zhang − *Alexandra Navrotsky Institute for Experimental Thermodynamics and The Gene and Linda Voiland School of Chemical Engineering and Bioengineering, Washington State University, Pullman, Washington 99164, United States*

Jeffrey A. Eakin − *The Gene and Linda Voiland School of Chemical Engineering and Bioengineering, Washington State University, Pullman, Washington 99164, United States*

Martinus Dewa − *School of Mechanical and Materials Engineering, Washington State University, Pullman, Washington 99164, United States*

Houqian Li − *The Gene and Linda Voiland School of Chemical Engineering and Bioengineering, Washington State University, Pullman, Washington 99164, United States*

Nan Li − *Center for Integrated Nanotechnologies, Los Alamos National Laboratory, Los Alamos, New Mexico 87545, United States*

Junming Sun − *The Gene and Linda Voiland School of Chemical Engineering and Bioengineering, Washington State University, Pullman, Washington 99164, United States;* orcid.org/0000-0002-0071-9635

Su Ha − *The Gene and Linda Voiland School of Chemical Engineering and Bioengineering, Washington State University, Pullman, Washington 99164, United States*

Cornelius F. Ivory − *The Gene and Linda Voiland School of Chemical Engineering and Bioengineering, Washington State University, Pullman, Washington 99164, United States*

Yong Wang − *The Gene and Linda Voiland School of Chemical Engineering and Bioengineering, Washington State University, Pullman, Washington 99164, United States; Institute for Integrated Catalysis, Pacific Northwest National Laboratory, Richland, Washington 99352, United States;* orcid.org/0000-0002-8460-7410

Hongwu Xu − *Earth and Environmental Sciences Division, Los Alamos National Laboratory, Los Alamos, New Mexico 87545, United States*

Complete contact information is available at: https://pubs.acs.org/10.1021/acsami.1c10021

Notes

The authors declare no competing financial interest.

■ ACKNOWLEDGMENTS

This work was supported by the institutional funds from the Gene and Linda Voiland School of Chemical Engineering Bioengineering and Alexandra Navrotsky Institute for Experimental Thermodynamics at Washington State University. C.B.C. was supported by the Achievement Rewards for College Scientists (ARCS) Fellowship from the ARCS Seattle Chapter and the Natural Resource Conservation Fund (NRCEF) through the Office of Research at WSU. J.A.E. was supported by the Department of Energy and National Nuclear Science Administration under Award Number DE-NA0003763. This work was performed, in part, at the Center for Integrated Nanotechnologies, an Office of Science User Facility operated for the U.S. Department of Energy (DOE) Office of Science. Los Alamos National Laboratory, an affirmative action equal opportunity employer, is managed by Triad National Security, LLC for the U.S. Department of Energy's NNSA, under contract 89233218CNA000001.

■ DEDICATION

This study is dedicated to a friend and colleague of D.W., *Prof. Chia-Kuang (Frank) Tsung*, Associate Professor of Chemistry at *Boston College*, who passed away on January 5, 2021, from complications due to COVID-19.

■ REFERENCES

(1) Ronchi, R. M.; Arantes, J. T.; Santos, S. F. Synthesis, Structure, Properties and Applications of MXenes: Current Status and Perspectives. *Ceram. Int.* **2019**, *45* (15), 18167−18188.

(2) Xiong, D.; Li, X.; Bai, Z.; Lu, S. Recent Advances in Layered $Ti_3C_2T_x$ MXene for Electrochemical Energy Storage. *Small* **2018**, *14* (17), 1703419.

(3) Gao, G.; O'Mullane, A. P.; Du, A. 2D MXenes: A New Family of Promising Catalysts for the Hydrogen Evolution Reaction. *ACS Catal.* **2017**, *7* (1), 494−500.
(4) Zhang, Y.; Wang, L.; Zhang, N.; Zhou, Z. Adsorptive Environmental Applications of MXene Nanomaterials: A Review. *RSC Adv.* **2018**, *8* (36), 19895−19905.
(5) Shahzad, F.; Alhabeb, M.; Hatter, C. B.; Anasori, B.; Hong, S. M.; Koo, C. M.; Gogotsi, Y. Electromagnetic Interference Shielding with 2D Transition Metal Carbides (MXenes). *Science (Washington, DC, U. S.)* **2016**, *353* (6304), 1137−1140.
(6) Xu, F.; Zhang, D.; Liao, Y.; Wang, G.; Shi, X.; Zhang, H.; Xiang, Q. Synthesis and Photocatalytic H_2-Production Activity of Plasma-Treated $Ti_3C_2T_x$ MXene Modified Graphitic Carbon Nitride. *J. Am. Ceram. Soc.* **2020**, *103* (2), 849−858.
(7) Pang, J.; Mendes, R. G.; Bachmatiuk, A.; Zhao, L.; Ta, H. Q.; Gemming, T.; Liu, H.; Liu, Z.; Rummeli, M. H. Applications of 2D MXenes in Energy Conversion and Storage Systems. *Chem. Soc. Rev.* **2019**, *48* (1), 72−133.
(8) Anasori, B.; Lukatskaya, M. R.; Gogotsi, Y. 2D Metal Carbides and Nitrides (MXenes) for Energy Storage. *Nat. Rev. Mater.* **2017**, *2*, 16098.
(9) Naguib, M.; Kurtoglu, M.; Presser, V.; Lu, J.; Niu, J.; Heon, M.; Hultman, L.; Gogotsi, Y.; Barsoum, M. W. Two-Dimensional Nanocrystals Produced by Exfoliation of Ti_3AlC_2. *Adv. Mater.* **2011**, *23* (37), 4248−4253.
(10) Seredych, M.; Shuck, C. E.; Pinto, D.; Alhabeb, M.; Precetti, E.; Deysher, G.; Anasori, B.; Kurra, N.; Gogotsi, Y. High-Temperature Behavior and Surface Chemistry of Carbide MXenes Studied by Thermal Analysis. *Chem. Mater.* **2019**, *31* (9), 3324−3332.
(11) Thakur, R.; VahidMohammadi, A.; Moncada, J.; Adams, W. R.; Chi, M.; Tatarchuk, B.; Beidaghi, M.; Carrero, C. A. Insights into the Thermal and Chemical Stability of Multilayered V_2CT_x MXene. *Nanoscale* **2019**, *11*, 10716−10726.
(12) Li, J.; Du, Y.; Huo, C.; Wang, S.; Cui, C. Thermal Stability of Two-Dimensional Ti_2C Nanosheets Thermal Stability of Two-Dimensional Ti_2C Nanosheets. *Ceram. Int.* **2015**, *41* (2), 2631−2635.
(13) Li, Z.; Wang, L.; Sun, D.; Zhang, Y.; Liu, B.; Hu, Q.; Zhou, A. Synthesis and Thermal Stability of Two-Dimensional Carbide MXene Ti_3C_2. *Mater. Sci. Eng., B* **2015**, *191* (C), 33−40.
(14) Wang, K.; Zhou, Y.; Xu, W.; Huang, D.; Wang, Z.; Hong, M. Fabrication and Thermal Stability of Two-Dimensional Carbide Ti_3C_2 Nanosheets. *Ceram. Int.* **2016**, *42* (7), 8419−8424.
(15) Wu, M.; Wang, B.; Hu, Q.; Wang, L.; Zhou, A. The Synthesis Process and Thermal Stability of V_2C MXene. *Materials* **2018**, *11* (11), 2112.
(16) Hu, Q.; Cao, X.; Li, Z.; Wang, L.; Zhou, A.; Gao, Y. Preparation of MXene-Cu_2O Nanocomposite and Effect on Thermal Decomposition of Ammonium Perchlorate. *Solid State Sci.* **2014**, *35*, 62−65.
(17) Cao, Y.; Deng, Q.; Liu, Z.; Shen, D.; Wang, T.; Huang, Q.; Du, S.; Jiang, N.; Lin, C. Te; Yu, J. Enhanced Thermal Properties of Poly(Vinylidene Fluoride) Composites with Ultrathin Nanosheets of MXene. *RSC Adv.* **2017**, *7* (33), 20494−20501.
(18) Han, M.; Yin, X.; Wu, H.; Hou, Z.; Song, C.; Li, X.; Zhang, L.; Cheng, L. Ti_3C_2 MXenes with Modified Surface for High-Performance Electromagnetic Absorption and Shielding in the X-Band. *ACS Appl. Mater. Interfaces* **2016**, *8* (32), 21011−21019.
(19) Zhang, H.; Wang, L.; Chen, Q.; Li, P.; Zhou, A.; Cao, X.; Hu, Q. Preparation, Mechanical and Anti-Friction Performance of MXene/Polymer Composites. *Mater. Des.* **2016**, *92*, 682−689.
(20) Wu, X.; Hao, L.; Zhang, J.; Zhang, X.; Wang, J.; Liu, J. Polymer-$Ti_3C_2T_x$ Composite Membranes to Overcome the Trade-off in Solvent Resistant Nanofiltration for Alcohol-Based System. *J. Membr. Sci.* **2016**, *515*, 175−188.
(21) Liu, Y.; Zhang, J.; Zhang, X.; Li, Y.; Wang, J. $Ti_3C_2T_x$ Filler Effect on the Proton Conduction Property of Polymer Electrolyte Membrane. *ACS Appl. Mater. Interfaces* **2016**, *8* (31), 20352−20363.
(22) Feng, A.; Yu, Y.; Jiang, F.; Wang, Y.; Mi, L.; Yu, Y.; Song, L. Fabrication and Thermal Stability of NH_4HF_2-Etched Ti_3C_2 MXene. *Ceram. Int.* **2017**, *43* (8), 6322−6328.
(23) Cockreham, C.; Zhang, X.; Li, H.; Hammond-Pereira, E.; Sun, J.; Saunders, S. R.; Wang, Y.; Xu, H.; Wu, D. Inhibition of AlF3·3H2O Impurity Formation in $Ti_3C_2T_x$ MXene Synthesis under a Unique CoF_x/HCl Etching Environment. *ACS Appl. Energy Mater.* **2019**, *2*, 8145.
(24) Schneider, C. A.; Rasband, W. S.; Eliceiri, K. W. NIH Image to ImageJ: 25 Years of Image Analysis. *Nat. Methods* **2012**, *9* (7), 671−675.
(25) Cockreham, C. B.; Zhang, X.; Lau, M. L.; Long, M.; Guo, X.; Xu, H.; Wu, D. Thermal Evolutions and Resulting Microstructural Changes in Kerogen-Rich Marcellus Shale. *ACS Earth Sp. Chem.* **2020**, *4* (12), 2461−2469.
(26) Zhang, X.; Cockreham, C. B.; Huang, Z.; Sun, H.; Yang, C.; Marin-Flores, O. G.; Wang, B.; Guo, X.; Ha, S.; Xu, H.; Wu, D. Thermodynamics of Water-Cationic Species-Framework Guest-Host Interactions within Transition Metal Ion-Exchanged Mordenite Relevant to Selective Anaerobic Oxidation of Methane to Methanol. *J. Phys. Chem. Lett.* **2020**, *11* (12), 4774−4784.
(27) Li, G.; Zhang, X.; Qiu, D.; Liu, Z.; Yang, C.; Cockreham, C. B.; Wang, B.; Fu, L.; Zhang, J.; Sudduth, B.; Guo, X.; Sun, H.; Huang, Z.; Qi, J.; Sun, J.; Ha, S.; Wang, Y.; Wu, D. Tuning Ni/Al Ratio to Enhance Pseudocapacitive Charge Storage Properties of Nickel−Aluminum Layered Double Hydroxide. *Adv. Electron. Mater.* **2019**, *5*, 1900215.
(28) Delong, X.; Yongqin, L.; Ying, J.; Longbao, Z.; Wenkui, G. Thermal Behavior of Aluminum Fluoride Trihydrate. *Thermochim. Acta* **2000**, *352*−*353*, 47−52.
(29) Delong, X.; Yongqin, L.; Ying, J.; Longbao, Z.; Wenkui, G. Thermal Behavior of Aluminum Fluoride Trihydrate. *Thermochim. Acta* **2000**, *352*−*353*, 47−52.
(30) Zhi, W.; Xiang, S.; Bian, R.; Lin, R.; Wu, K.; Wang, T.; Cai, D. Study of MXene-Filled Polyurethane Nanocomposites Prepared via an Emulsion Method. *Compos. Sci. Technol.* **2018**, *168*, 404−411.
(31) Shi, C.; Beidaghi, M.; Naguib, M.; Mashtalir, O.; Gogotsi, Y.; Billinge, S. J. L. Structure of Nanocrystalline Ti_3C_2 MXene Using Atomic Pair. *Phys. Rev. Lett.* **2014**, *112* (12), 125501.
(32) Alhabeb, M.; Maleski, K.; Anasori, B.; Lelyukh, P.; Clark, L.; Sin, S.; Gogotsi, Y. Guidelines for Synthesis and Processing of Two-Dimensional Titanium Carbide ($Ti_3C_2T_x$ MXene). *Chem. Mater.* **2017**, *29* (18), 7633−7644.
(33) Madsen, F. T.; Noesch, R. The Swelling Behaviour of Clay-Sulfate Rocks. In *7th ISRM Congrress*, Aachen, Germany, September 16−20, 1991.
(34) Hensen, E. J. M.; Smit, B. Why Clays Swell. *J. Phys. Chem. B* **2002**, *106* (49), 12664−12667.
(35) Célérier, S.; Hurand, S.; Garnero, C.; Morisset, S.; Benchakar, M.; Habrioux, A.; Chartier, P.; Mauchamp, V.; Findling, N.; Lanson, B.; Ferrage, E. Hydration of $Ti_3C_2T_x$ MXene: An Interstratification Process with Major Implications on Physical Properties. *Chem. Mater.* **2019**, *31* (2), 454−461.
(36) Liu, R.; Li, W. High-Thermal-Stability and High-Thermal-Conductivity $Ti_3C_2T_x$ MXene/Poly(Vinyl Alcohol) (PVA) Composites. *ACS Omega* **2018**, *3* (3), 2609−2617.
(37) Yan, P.; Zhang, R.; Jia, J.; Wu, C.; Zhou, A.; Xu, J.; Zhang, X. Enhanced Supercapacitive Performance of Delaminated Two-Dimensional Titanium Carbide/Carbon Nanotube Composites in Alkaline Electrolyte. *J. Power Sources* **2015**, *284*, 38−43.
(38) Han, Y.-H.; Deng, Q.; Huang, Q.; Du, S.; Zhou, X.; Li, Y.; Lee, J.; Wang, J.; Li, M. Facile Preparation of in situ Coated $Ti_3C_2T_x$/$Ni_{0.5}Zn_{0.5}Fe_2O_4$ Composites and Their Electromagnetic Performance. *RSC Adv.* **2017**, *7* (40), 24698−24708.
(39) Smykatz-Kloss, W.; Heide, K.; Klinke, W. Chapter 11: Applications of Thermal Methods in the Geosciences. In *Applications to Inorganic and Miscellaneous Materials: Handbook of Thermal Analysis and Calorimetry*; Brown, M. E., Gallagher, P. K., Eds.; Elsevier Science B.V., 2003; Vol. 2, pp 451−593;.
(40) Masumoto, H.; Kameda, J.; Arima, H.; Sugiyama, K.; Nagai, T.; Yamamoto, Y. Dehydroxylation Kinetics of Clay Minerals and Its Application to Friction Heating Along an Imbricate Thrust in an

https://doi.org/10.1021/acsami.1c10021
ACS Appl. Mater. Interfaces 2021, 13, 52125−52133

Accretionary Prism. *Geochem., Geophys., Geosyst.* **2018**, *19* (9), 2991−3003.
(41) Ghidiu, M.; Lukatskaya, M. R.; Zhao, M. Q.; Gogotsi, Y.; Barsoum, M. W. Conductive Two-Dimensional Titanium Carbide "clay" with High Volumetric Capacitance. *Nature* **2014**, *516* (7529), 78−81.
(42) Wang, X.; Garnero, C.; Rochard, G.; Magne, D.; Morisset, S.; Hurand, S.; Chartier, P.; Rousseau, J.; Cabioc'H, T.; Coutanceau, C.; Mauchamp, V.; Célérier, S. A New Etching Environment (FeF_3/HCl) for the Synthesis of Two-Dimensional Titanium Carbide MXenes: A Route towards Selective Reactivity: Vs. Water. *J. Mater. Chem. A* **2017**, *5* (41), 22012−22023.

https://doi.org/10.1021/acsami.1c10021
ACS Appl. Mater. Interfaces 2021, 13, 52125−52133